HII Regions

Osterbrock S2

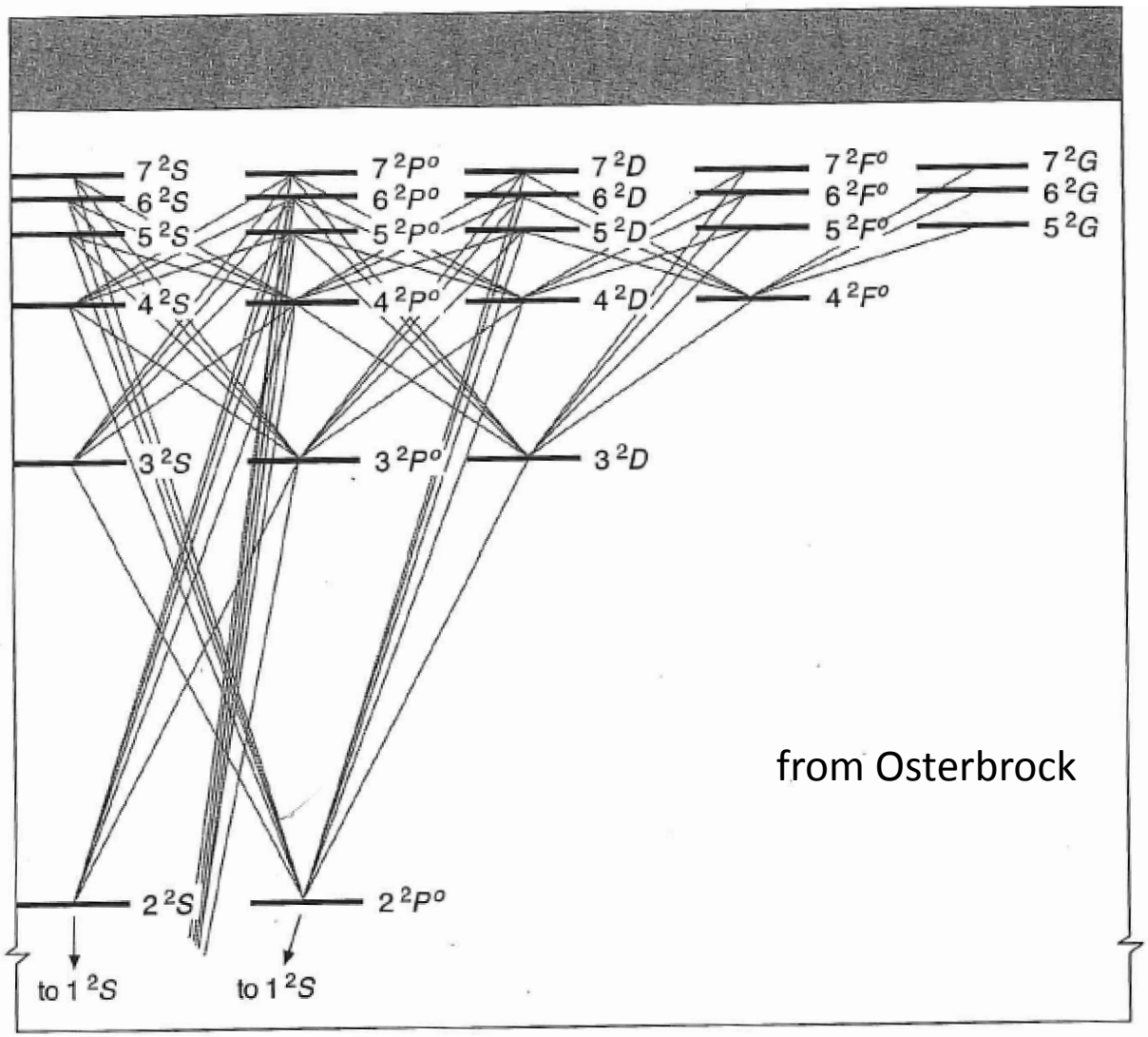

Figure 2.1

Partial energy-level diagram of H I, limited to $n \leq 7$ and $L \leq G$. Permitted radiative transitions to levels $n < 4$ are indicated by solid lines.

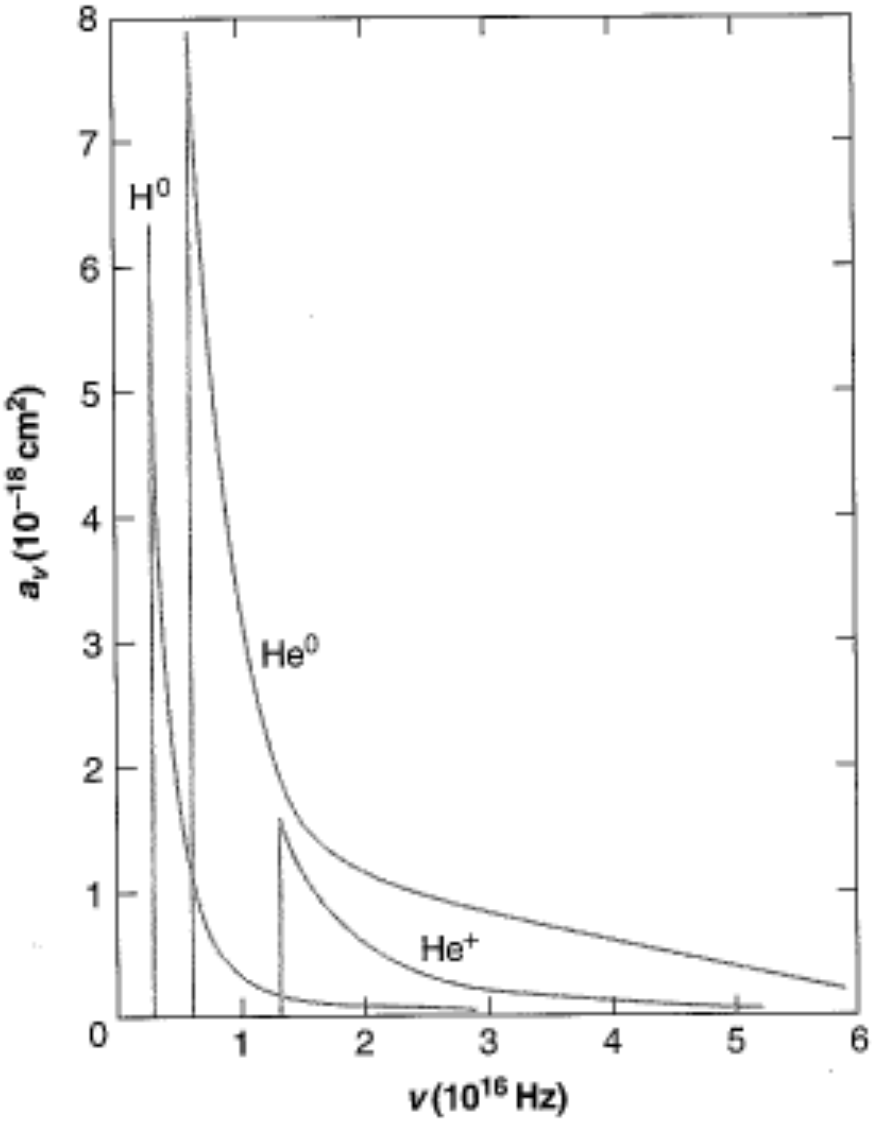

Ionization cross-section (Osterbrock)

Table 4.1. Collision Strengths for Excitation by Electrons

Number of p electrons	Ion	Levels		E_{jk}(eV)	$\Omega(j,k)$	$\Sigma_j A_{kj}(s^{-1})$
		Lower	Upper			
1,5	C II	$^2P_{1/2}$	$^2P_{3/2}$	0.0079	1.33	2.4×10^{-6}
	Ne II	$^2P_{3/2}$	$^2P_{1/2}$	0.097	0.37	8.6×10^{-3}
	Si II	$^2P_{1/2}$	$^2P_{3/2}$	0.036	7.7	2.1×10^{-4}
2	N II	$^3P_0$	$^3P_1$	0.0061	0.41	2.1×10^{-6}
		$^3P_0$	$^3P_2$	0.0163	0.28	7.5×10^{-6}
		$^3P_1$	$^3P_2$	0.0102	1.38	7.5×10^{-6}
		^3P	$^1D_2$	1.90	2.99	4.0×10^{-3}
		^3P	$^1S_0$	4.05	0.36	1.1
	O III	$^3P_0$	$^3P_1$	0.014	0.39	2.6×10^{-5}
		$^3P_0$	$^3P_2$	0.038	0.21	9.8×10^{-5}
		$^3P_1$	$^3P_2$	0.024	0.95	9.8×10^{-5}
		^3P	$^1D_2$	2.51	2.50	2.8×10^{-2}
		^3P	$^1S_0$	5.35	0.30	1.8
3	O II	$^4S_{3/2}$	$^2D_{5/2}$	3.32	0.88	4.2×10^{-5}
		$^4S_{3/2}$	$^2D_{3/2}$	3.32	0.59	1.8×10^{-4}
		$^2D_{3/2}$	$^2D_{5/2}$	0.0025	1.16	4.2×10^{-5}

from Spitzer

Table 5.1. Fluxes of ionizing photons $S_0 = N_{LyC}(\mathrm{H\,I})$ and $S_1 = N_{LyC}(\mathrm{He\,I})$ in the hydrogen and helium Lyman continua for various types of hot stars with solar abundances, from Schaerer & de Koter [456].

Sp. type	V(dwarf)			III(giant)			I(supergiant)		
	$\log T_{eff}$ K	$\log S_0$ s^{-1}	$\log S_1$ s^{-1}	$\log T_{eff}$ K	$\log S_0$ s^{-1}	$\log S_1$ s^{-1}	$\log T_{eff}$ K	$\log S_0$ s^{-1}	$\log S_1$ s^{-1}
O3	4.710	49.85	49.42	4.707	49.97	49.52	4.705	50.09	49.63
O4	4.687	49.68	49.23	4.683	49.84	49.38	4.678	50.02	49.56
O4.5	4.676	49.58	49.12	4.670	49.78	49.32	4.665	49.98	49.53
O5	4.664	49.48	49.01	4.657	49.71	49.25	4.650	49.94	49.47
O5.5	4.652	49.38	48.86	4.644	49.64	49.16	4.636	49.88	49.35
O6	4.639	49.28	48.75	4.630	49.56	49.05	4.620	49.81	49.24
O6.5	4.626	49.17	48.62	4.615	49.47	48.91	4.604	49.73	49.12
O7	4.613	49.05	48.44	4.601	49.36	48.75	4.588	49.64	48.91
O7.5	4.599	48.93	48.25	4.585	49.24	48.53	4.571	49.53	48.65
O8	4.585	48.80	48.05	4.569	40.09	48.14	4.553	49.42	48.37
O8.5	4.570	48.64	47.74	4.553	48.94	47.80	4.534	49.29	48.05
O9	4.555	48.46	47.37	4.536	48.76	47.40	4.515	49.12	47.67
O9.5	4.539	48.25	46.92	4.518	48.56	46.95	4.495	48.90	47.21
B0	4.523	48.02	46.41	4.499	48.33	46.47	–	–	–
B0.5	4.506	47.77	45.86	4.479	48.11	46.03	–	–	–

from Lequeux

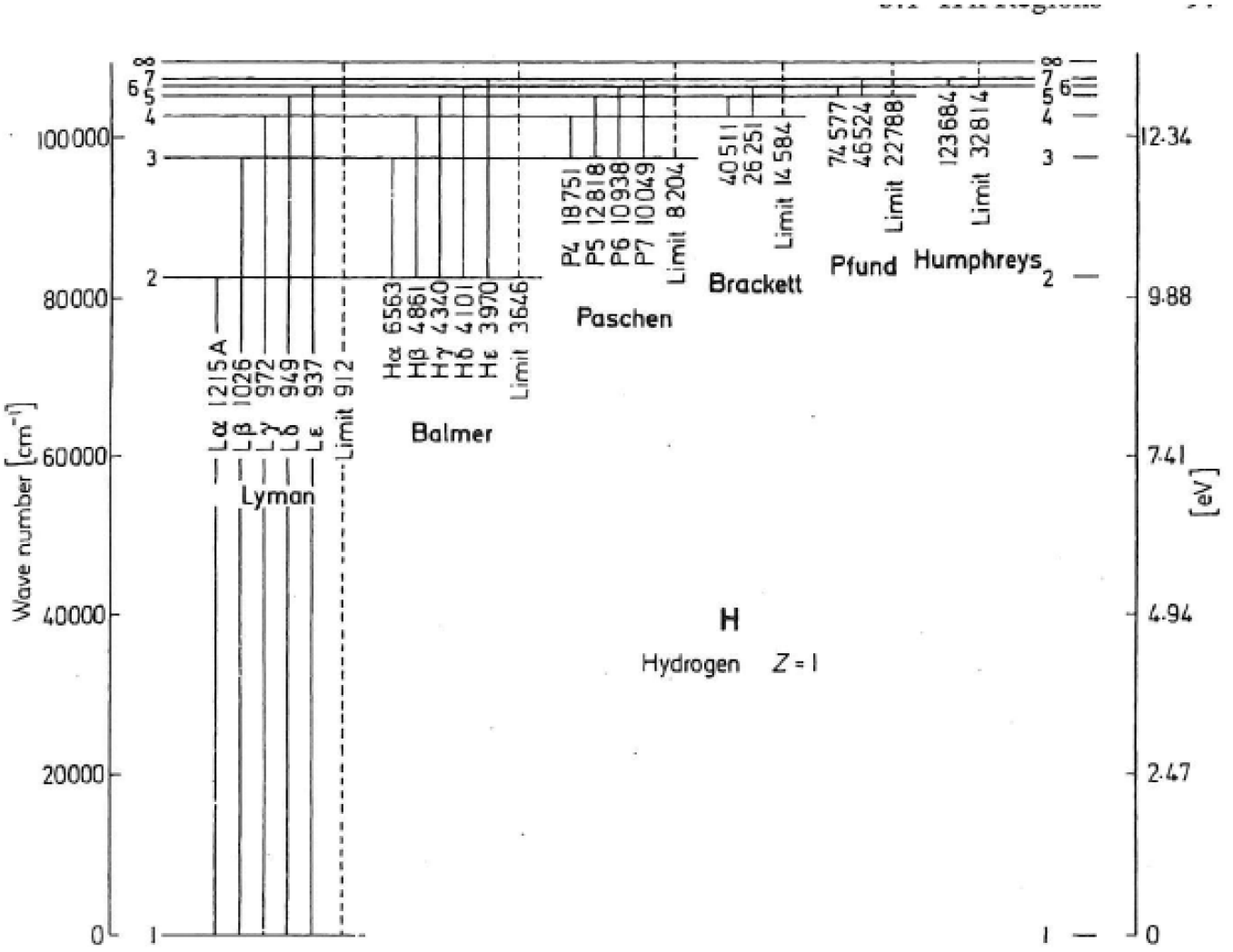

Fig. 5.5. Energy diagram for the hydrogen atom, with the different series designated. The principal quantum number n is indicated to the left of each level. The scale of the ordinate is in wave numbers, $1/\lambda$, and should be multiplied by hc in order to obtain the energies. From Lang [299].

from Lequeux

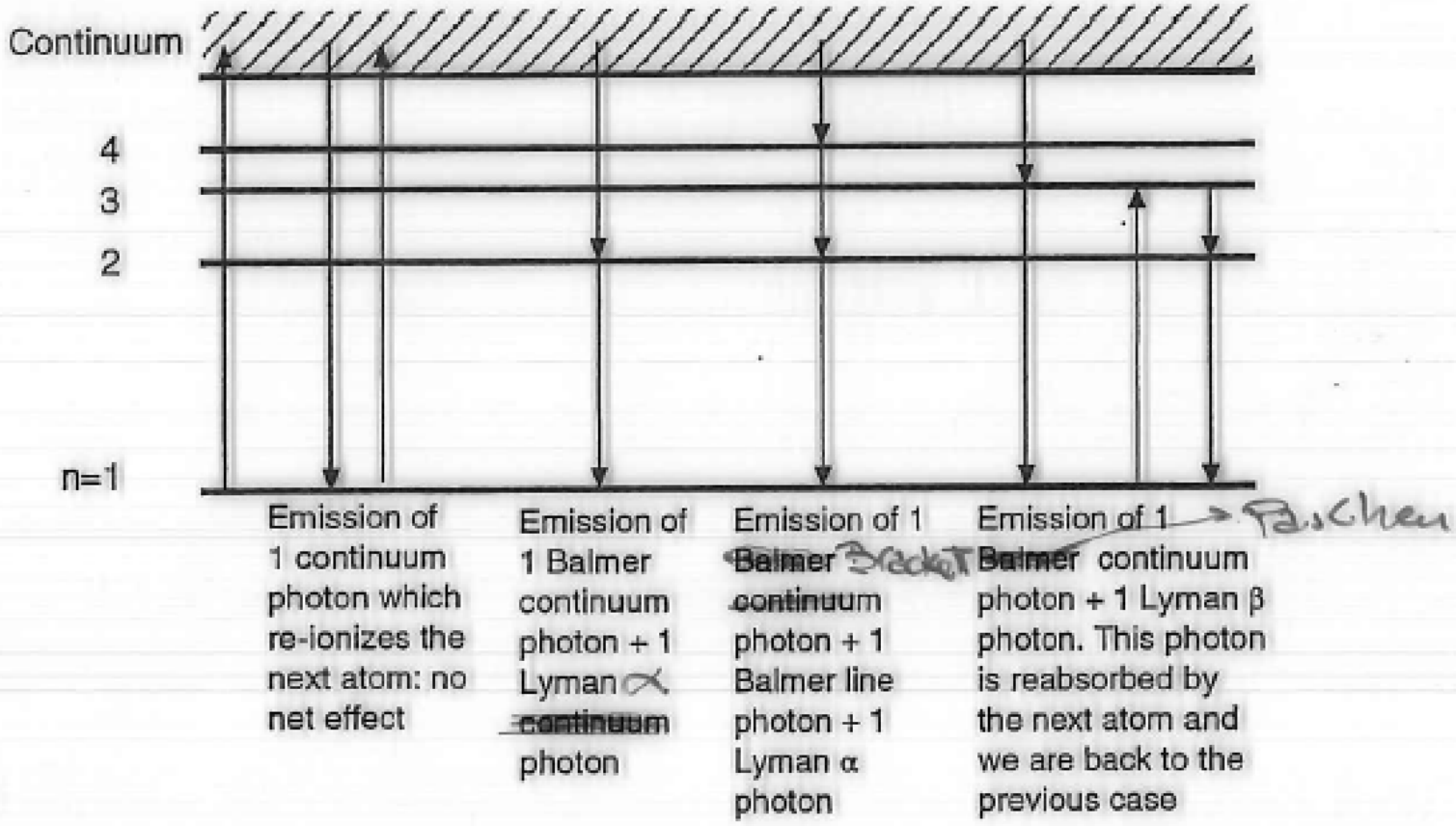

Fig. 5.6. Schematic showing that every recombination of hydrogen in an H II region produces a Balmer photon in case B.

from Lequeux

Table 4.1

H I recombination lines (Case A, low-density limit)

	T			
	2,500 K	5,000 K	10,000 K	20,000 K
$4\pi j_{H\beta}/n_e n_p$ (erg cm^3 s^{-1})	2.70×10^{-25}	1.54×10^{-25}	8.30×10^{-26}	4.21×10^{-26}
$\alpha_{H\beta}^{eff}$ (cm^3 s^{-1})	6.61×10^{-14}	3.78×10^{-14}	2.04×10^{-14}	1.03×10^{-14}
Balmer-line intensities relative to Hβ				
$j_{H\alpha}/j_{H\beta}$	3.42	3.10	2.86	2.69
$j_{H\gamma}/j_{H\beta}$	0.439	0.458	0.470	0.485
$j_{H\delta}/j_{H\beta}$	0.237	0.250	0.262	0.271
$j_{H\varepsilon}/j_{H\beta}$	0.143	0.153	0.159	0.167
$j_{H8}/j_{H\beta}$	0.0957	0.102	0.107	0.112
$j_{H9}/j_{H\beta}$	0.0671	0.0717	0.0748	0.0785
$j_{H10}/j_{H\beta}$	0.0488	0.0522	0.0544	0.0571
$j_{H15}/j_{H\beta}$	0.0144	0.0155	0.0161	0.0169
$j_{H20}/j_{H\beta}$	0.0061	0.0065	0.0068	0.0071
Lyman-line intensities relative to Hβ				
$j_{L\alpha}/j_{H\beta}$	33.0	32.5	32.7	34.0
Paschen-line intensities relative to Hβ				
$j_{P\alpha}/j_{H\beta}$	0.684	0.562	0.466	0.394
$j_{P\beta}/j_{H\beta}$	0.267	0.241	0.216	0.196
$j_{P\gamma}/j_{H\beta}$	0.134	0.126	0.118	0.110
$j_{P8}/j_{H\beta}$	0.0508	0.0497	0.0474	0.0452
$j_{P10}/j_{H\beta}$	0.0258	0.0251	0.0239	0.0228
$j_{P15}/j_{H\beta}$	0.00750	0.00721	0.00691	0.00669
$j_{P20}/j_{H\beta}$	0.00310	0.00300	0.00290	0.00280

- Case A, nebula optically thin to Lyman photons (faint)
- Osterbrock

Table 4.2

H I recombination lines (Case B, low-density limit)

	T			
	2,500 K	5,000 K	10,000 K	20,000 K
$4\pi j_{H\beta}/n_e n_p$ (erg cm^3 s^{-1})	3.72×10^{-25}	2.20×10^{-25}	1.24×10^{-25}	6.62×10^{-26}
$\alpha^{eff}_{H\beta}$ (cm^3 s^{-1})	9.07×10^{-14}	5.37×10^{-14}	3.03×10^{-14}	1.62×10^{-14}
Balmer-line intensities relative to Hβ				
$j_{H\alpha}/j_{H\beta}$	3.30	3.05	2.87	2.76
$j_{H\gamma}/j_{H\beta}$	0.444	0.451	0.466	0.474
$j_{H\delta}/j_{H\beta}$	0.241	0.249	0.256	0.262
$j_{H\epsilon}/j_{H\beta}$	0.147	0.153	0.158	0.162
$j_{H8}/j_{H\beta}$	0.0975	0.101	0.105	0.107
$j_{H9}/j_{H\beta}$	0.0679	0.0706	0.0730	0.0744
$j_{H10}/j_{H\beta}$	0.0491	0.0512	0.0529	0.0538
$j_{H15}/j_{H\beta}$	0.0142	0.0149	0.0154	0.0156
$j_{H20}/j_{H\beta}$	0.0059	0.0062	0.0064	0.0065
Paschen-line intensities relative to Hβ				
$j_{P\alpha}/j_{H\beta}$	0.528	0.427	0.352	0.293
$j_{P\beta}/j_{H\beta}$	0.210	0.187	0.165	0.146
$j_{P\gamma}/j_{H\beta}$	0.1060	0.0991	0.0906	0.0820
$j_{P\delta}/j_{H\beta}$	0.0410	0.0392	0.0368	0.0343
$j_{P10}/j_{H\beta}$	0.0207	0.0199	0.0185	0.0172
$j_{P15}/j_{H\beta}$	0.00589	0.00571	0.00530	0.00501
$j_{P20}/j_{H\beta}$	0.00240	0.00240	0.00220	0.00210
Brackett-line intensities relative to Hβ				
$j_{Br\alpha}/j_{H\beta}$	0.1447	0.1091	0.0834	0.0640
$j_{Br\beta}/j_{H\beta}$	0.0709	0.0578	0.0471	0.0380
$j_{Br\gamma}/j_{H\beta}$	0.0387	0.0332	0.0281	0.0237
$j_{Br\delta}/j_{H\beta}$	0.0248	0.0216	0.0186	0.0157
$j_{Br10}/j_{H\beta}$	0.01193	0.01065	0.00920	0.00796
$j_{Br15}/j_{H\beta}$	0.00317	0.00295	0.00263	0.00231
$j_{Br20}/j_{H\beta}$	0.00127	0.00124	0.00109	0.00097

- Case B, nebula is optically thick (more typical of observed nebulae)

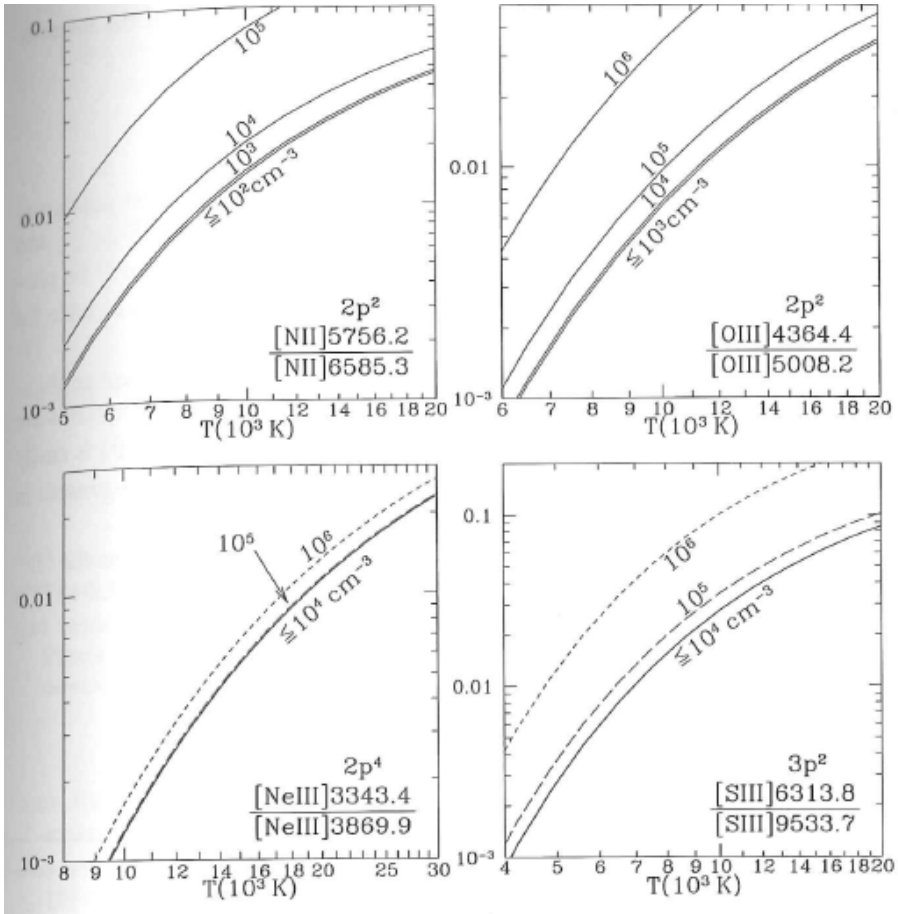

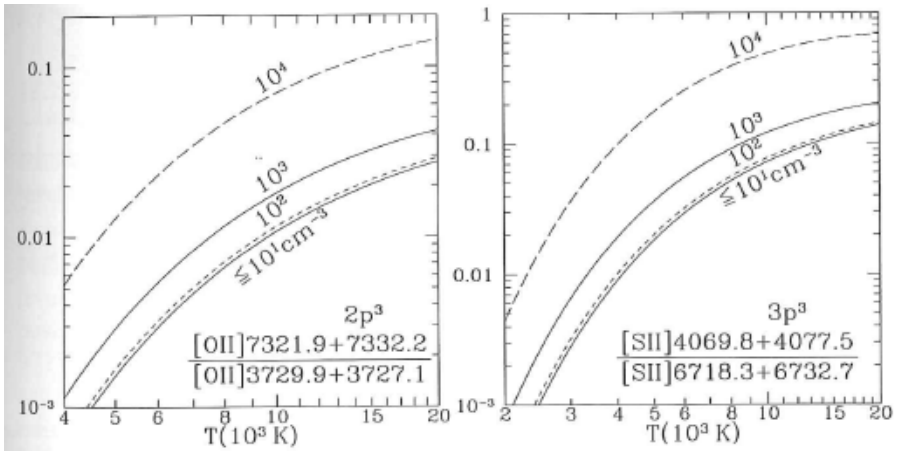

Figure 18.2 Line ratios that are useful as temperature diagnostics (see text). Curves are labeled by n_e (cm^{-3}). For each ion, the low density limit is shown, as well as results for higher densities, showing deviations from the low density behavior.

from Draine's book

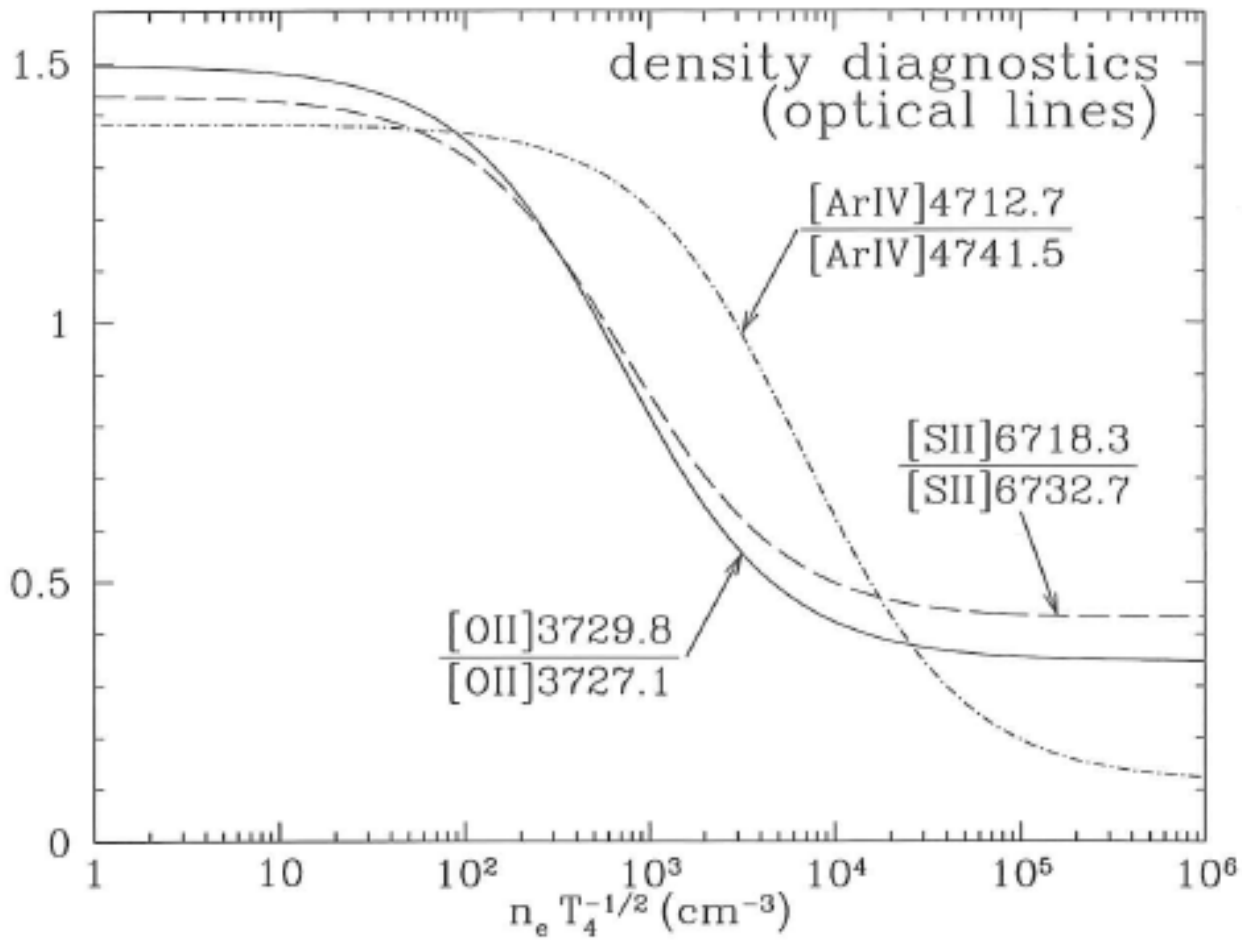

Figure 18.4 [O II], [S II], and [Ar IV] optical line intensity ratios useful for density determination. Wavelengths are in vacuo.

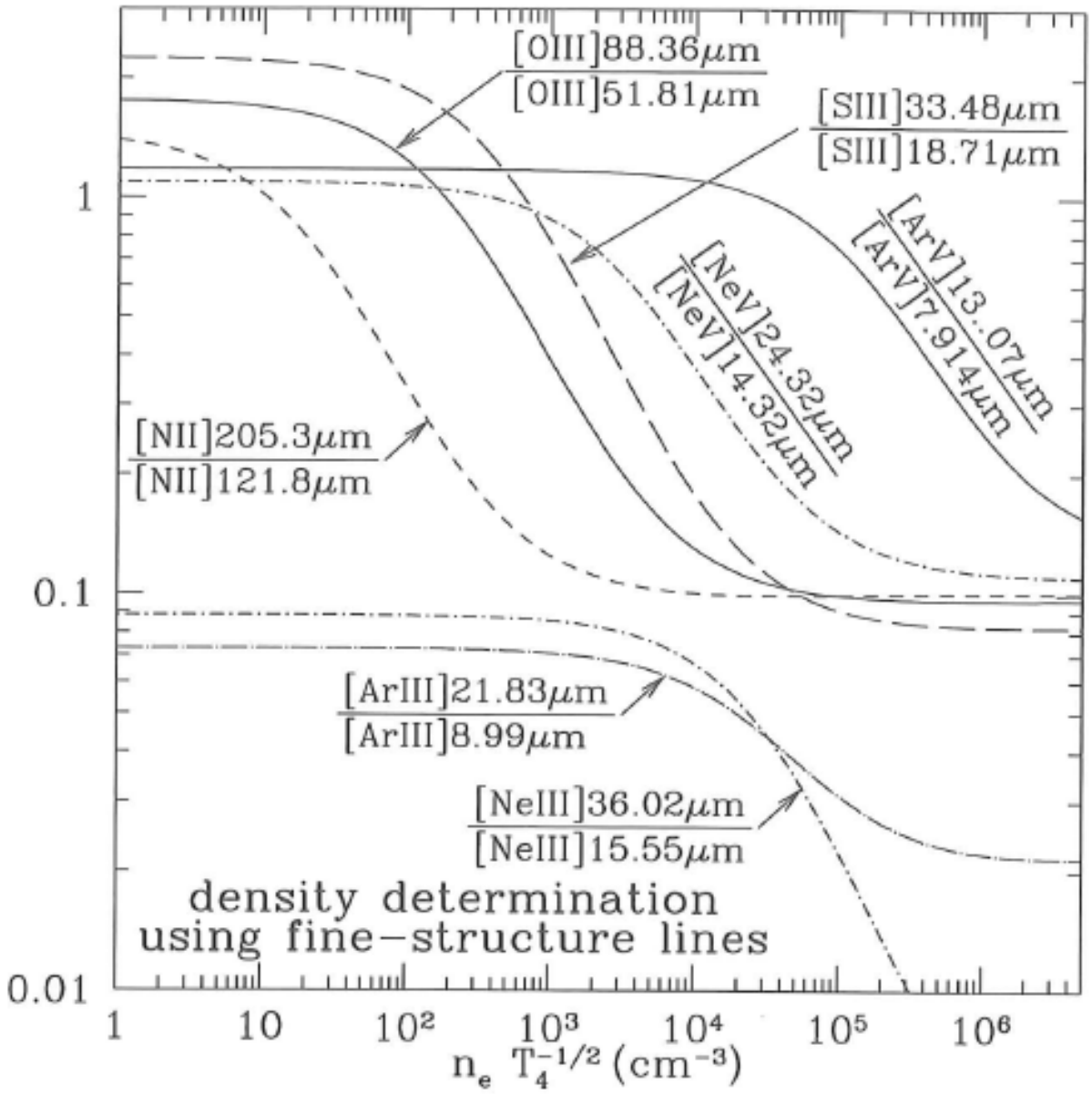

Figure 18.5 Fine-structure line ratios that can be used for density determination (see text).

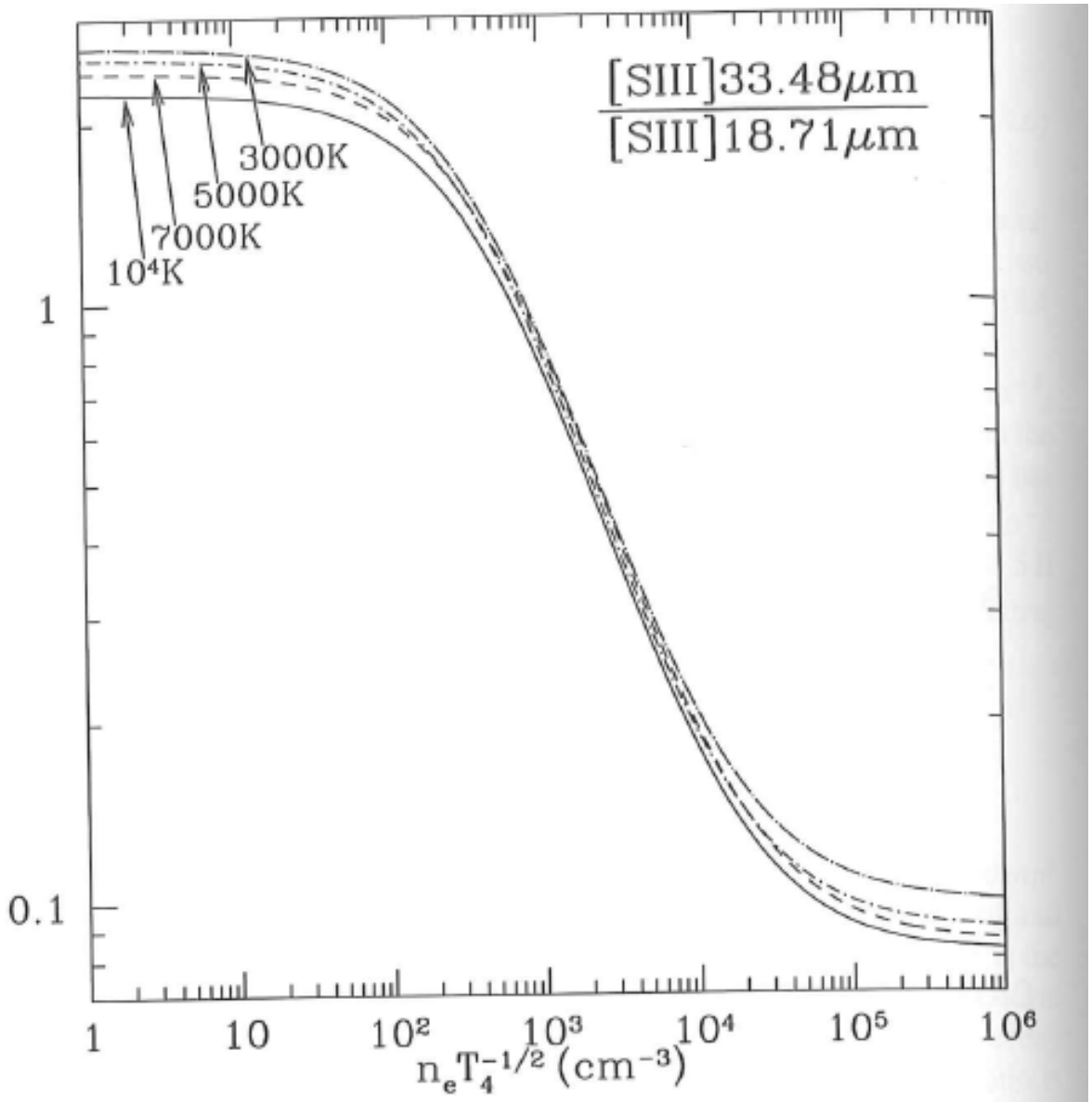

Figure 18.6 [S III]33.48 μm/[S III]18.71 μm as a function of $n_e/\sqrt{T_e}$, for four values of T_e. As the temperature is lowered, the line ratio rises both at low density and at high density.

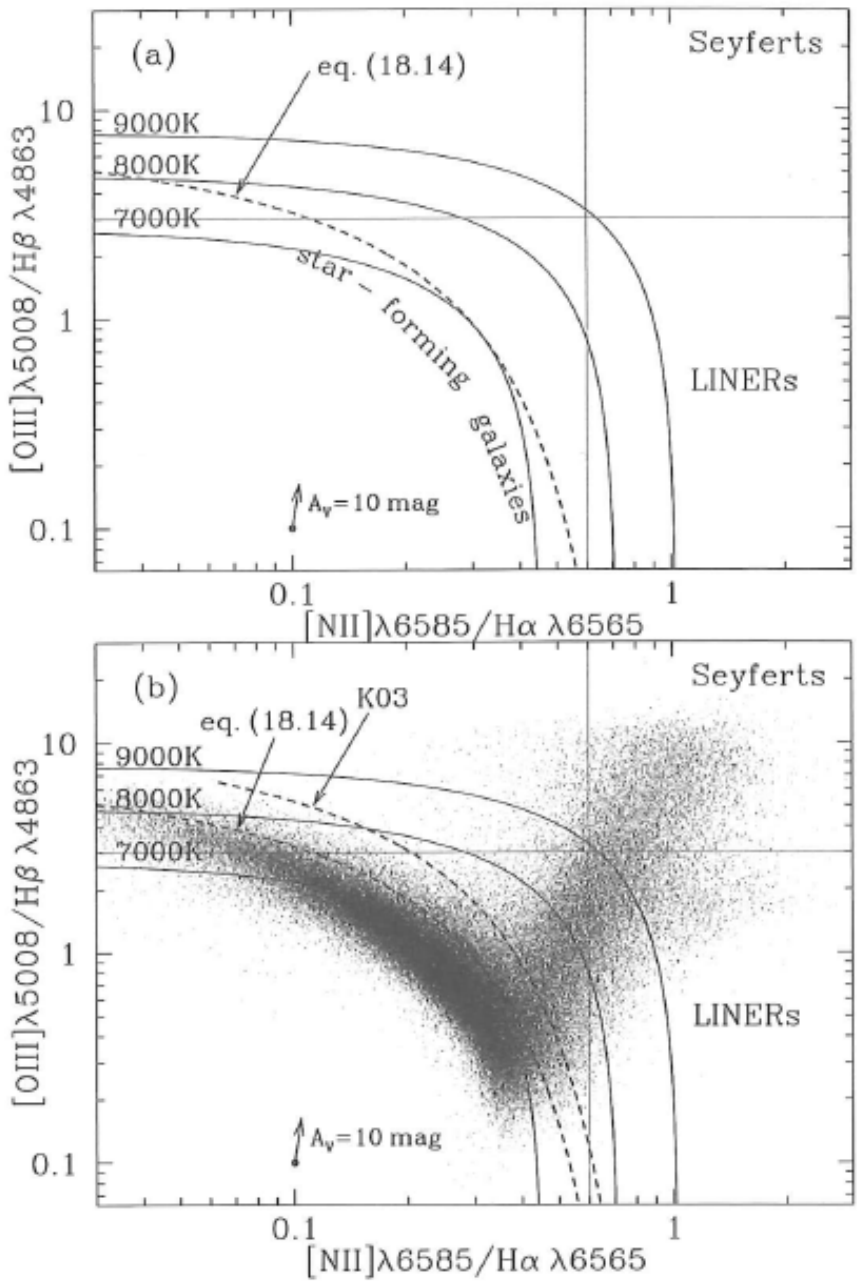

Figure 18.7 The so-called "BPT" diagram (Baldwin et al. 1981) showing [O III]5008/Hβ vs [N II]6585/Hα. The "reddening vector" shows the displacement on the plot due to reddening by Milky Way dust with $A_V = 10$ mag – it is clear that the BPT diagram is almost completely unaffected by reddening. (a) Solid curves show emission ratios calculated for gas with solar abundances, for three gas temperatures. Along each curve the oxygen and nitrogen vary from singly ionized at the bottom, to doubly ionized at the upper left. (b) Line ratios for 122514 galaxies in SDSS DR7 with S/N> 5. The curve labeled K03 is the boundary proposed by Kauffmann et al. (2003) to separate star-forming galaxies from AGN. Eq. (18.14) shows an improved boundary. 70.0% of the galaxies fall in the star-forming region defined by Eq. 18.14. 12.8% fall in the AGN region defined by [N II]6585/H$\alpha > 0.6$.

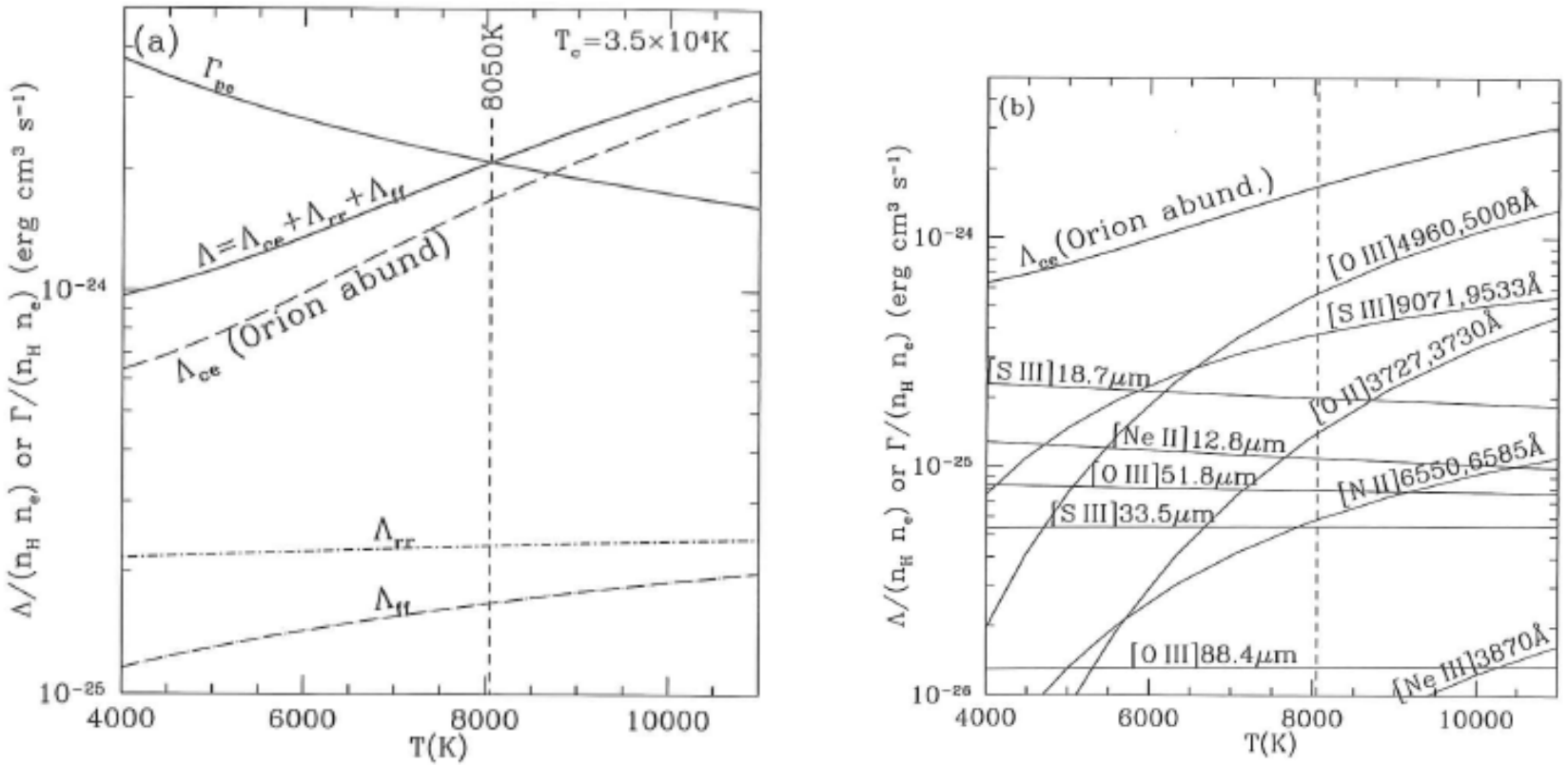

Figure 27.1 (a) Photoelectric heating function Γ_{pe} and radiative cooling function Λ as functions of gas temperature T in an H II region with Orion-like abundances and density $n_{\rm H} = 4000\,{\rm cm}^{-3}$. Heating and cooling balance at $T \approx 8050$ K. (b) Contributions of individual lines to Λ_{ce}.

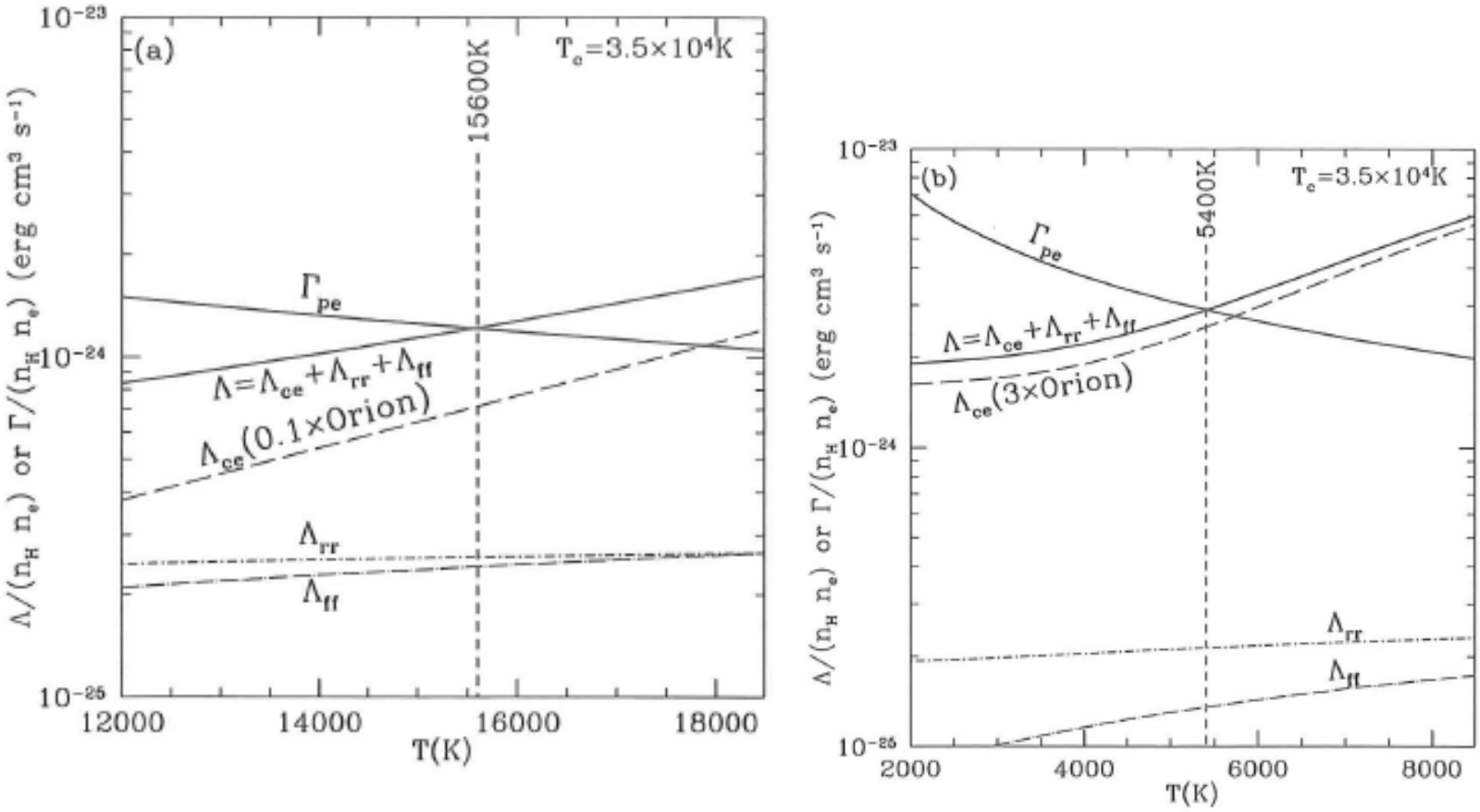

Figure 27.2 (a) Photoelectric heating function Γ_{pe} and radiative cooling function Λ as functions of temperature T in an H II region with abundances that are (a) only 10%, or (b) enhanced by a factor of 3 relative to the Orion Nebula. A density $n_{\rm H} = 4000\,{\rm cm}^{-3}$ is assumed. Thermal equilibrium occurs for $T \approx 15600$ K and ~ 5400 K for the two cases.

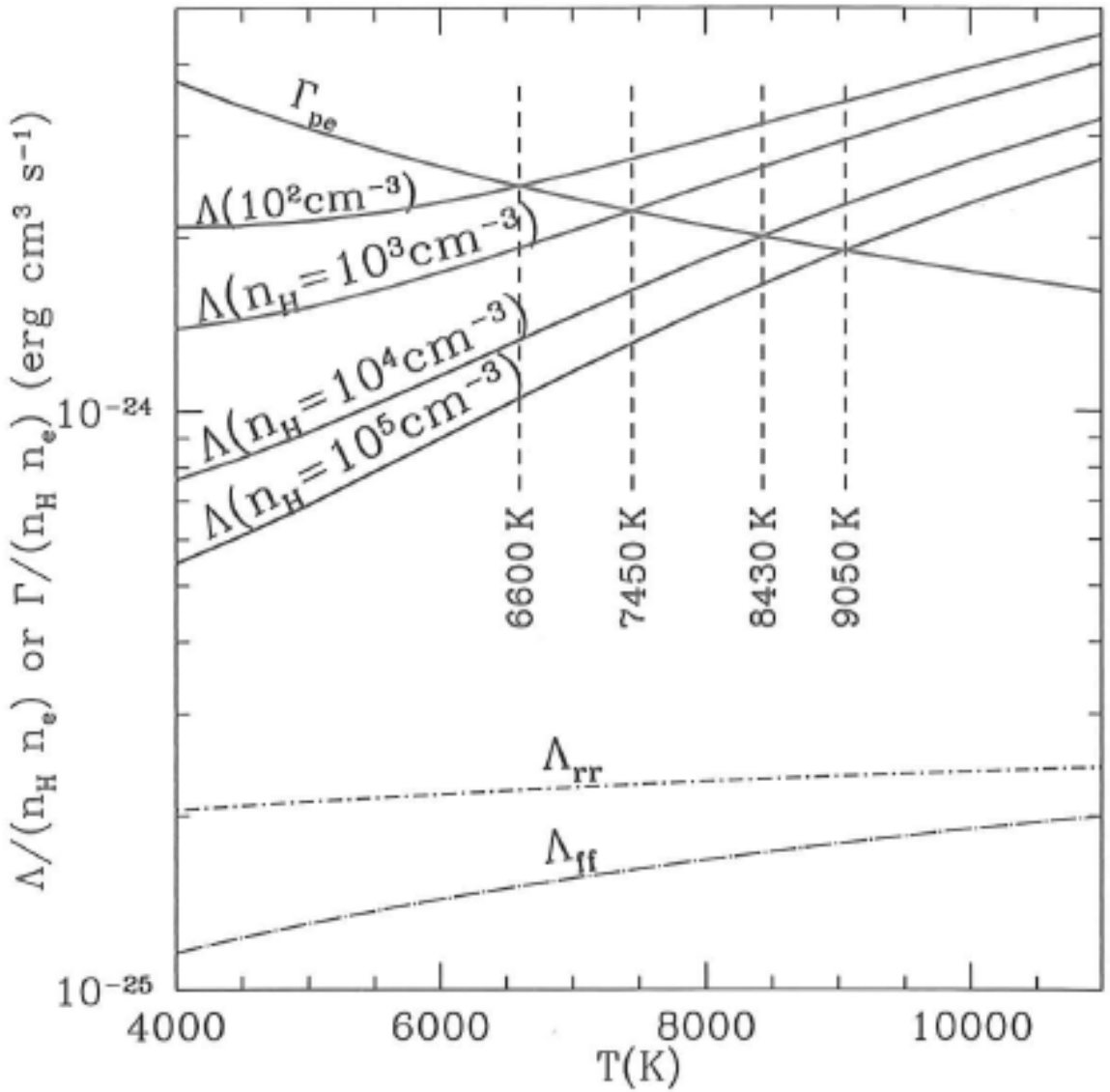

Figure 27.3 Cooling function $\Lambda(T)$ for different densities $n_{\rm H}$. The gas is assumed to have Orion-like abundances and ionization conditions. As the gas density is varied from 10^2 cm^{-3} to 10^5 cm^{-3}, the equilibrium temperature varies from 6600 K to 9050 K, because of collisional deexcitation of excited states.